

Preparation and evaluation of amido poly amine surfactant based on Melia azedarach seeds oil as corrosion inhibitor of C-steel in 2.0 M HCl pickling medium

Asmaa A. I. Ali & Wagdy I. A. El-DougDoug

To cite this article: Asmaa A. I. Ali & Wagdy I. A. El-DougDoug (2017) Preparation and evaluation of amido poly amine surfactant based on Melia azedarach seeds oil as corrosion inhibitor of C-steel in 2.0 M HCl pickling medium, Green Chemistry Letters and Reviews, 10:4, 346-358, DOI: [10.1080/17518253.2017.1385857](https://doi.org/10.1080/17518253.2017.1385857)

To link to this article: <https://doi.org/10.1080/17518253.2017.1385857>



© 2017 The Author(s). Published by Informa UK Limited, trading as Taylor & Francis Group



Published online: 25 Oct 2017.



Submit your article to this journal [↗](#)



Article views: 143



View related articles [↗](#)



View Crossmark data [↗](#)

Preparation and evaluation of amido poly amine surfactant based on *Melia azedarach* seeds oil as corrosion inhibitor of C-steel in 2.0 M HCl pickling medium

Asmaa A. I. Ali and Wagdy I. A. El-DougDoug

Chemistry Department, Faculty of Science, Benha University, Benha, Egypt

ABSTRACT

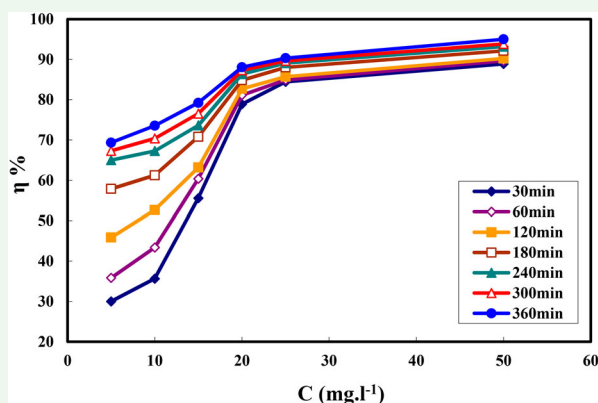
Oil of *Melia azedarach* seeds (MA-oil) was extracted and modified in the form of amido poly amine surfactant (MA-amido surfactant). The surface active properties of the new MA-amido surfactant were analyzed. Corrosion inhibition of C-steel in 2.0 M HCl by MA-amido surfactant was investigated using weight loss (WL), potentiodynamic polarization (PDP) and electrochemical impedance spectroscopy (EIS). The results indicated that the corrosion of C-steel was obviously reduced. PDP curves showed that the MA-amido surfactant behaves as a mixed-type inhibitor. The adsorption process at the C-steel surface obeys Langmuir adsorption isotherm model. The activation and thermodynamic parameters of the adsorption were evaluated and discussed. The protective film at the metal surface was characterized by a scanning electron microscope (SEM).

ARTICLE HISTORY

Received 8 June 2017
Accepted 25 September 2017

KEYWORDS

C-steel; adsorption; EIS; potentiodynamic polarization; synthesis of MA-amido surfactant



1. Introduction

Petroleum oil industry is one of the most important industries around the world. C-steel is the major constituent of the pipes and tanks used in this industry. Corrosion of the walls of pipes and tanks is the main problem facing this industry during its different working stages, especially mining, pipelines, refining, petroleum production, etc. Corrosion arises due to the presence of mineral compounds in crude oil beside other factors related to the working processes such as purity of working water and temperature (1). It results in the formation of rust and scale on the petroleum containers, which can be removed using hydrochloric acid. So problems may arise if the acid reacts with the C-steel,

causing corrosion damage. Using the corrosion inhibitors is one of the most important methods to protect the metal from damage.

Many groups of synthetic organic compounds have been reported to inhibit the effects of the acid corrosion on C-steel (2–8). These compounds generally contain aromatic rings and π -bonds beside oxygen, nitrogen and/or sulfur groups, which are efficient corrosion inhibitors in acid solutions. Among these compounds are surfactants, which are used as acid corrosion inhibitors for C-steel (9–12).

Current corrosion studies are focused on “green corrosion inhibitors,” that showed good inhibition efficiency with low risk of environmental pollution. The term “green

inhibitor” or “ecofriendly inhibitor” refers to substances that are biocompatible such as plant extracts (13). The inhibition potential of natural products (derived from different plant parts) towards the metal corrosion was being studied, which show excellent corrosion protection. Many green corrosion inhibitors originated from different plant sources were reported for C-steel protection in acidic media (14–18). Protective film stability at the metal surface depends on: physico-chemical properties of the inhibitor molecules, the type of aggressive media and the nature of the interaction between the d-orbital of the metal and the p-orbital of the inhibitors.

Recently, a green synthetic route for obtaining various plant derivatives to be used as a corrosion inhibitor has been reported in the literature (19, 20). No reported literature is available for using the oil of *Melia azedarach* seeds or its derivatives for the corrosion control of C-steel in any corrosive media. The major fatty acids of MA-oil are oleic, linoleic, palmitic and stearic acids (21, 22). The goal of this paper was to investigate the inhibitory effect of the new MA-amido surfactant, on the corrosion of C-steel in 2.0 M HCl via different techniques such as weight loss (WL), potentiodynamic polarization (PDP) technique, electrochemical impedance spectroscopy (EIS) and scanning electron microscope (SEM). The *Melia azedarach* seeds were collected from one of the existing agricultural fields in Menoufia, Egypt.

2. Experimental

2.1. Materials

Analytical-grade hydrochloric acid (37%), 40/60°C petroleum ether, KOH, acetone, methyl alcohol and tetraethylenepentamine (Merck) were used as received without any further purification. The working electrode was C-steel specimen with the following composition (wt %): C: 0.28, Mn: 1.25, P: 0.04, S: 0.05 and Fe: balance. The tested C-steel was previously worked in the Cairo.Co. for petroleum pipelines’ transportation.

2.2. Preparation and characterization of the MA-amido surfactant

2.2.1. Extraction of the MA-oil

The dried seeds of MA were pulverized to fine powder using electric grinder. The crude oil of MA-seeds was obtained and converted to its mixed fatty acid by the alkali hydrolysis, and then converted to fatty acids methyl ester according to (23, 24). The major fatty acids methyl ester was determined using GC – Mass Spectrum analysis Perkin elmer clarus 580 s (MS)/650 s. The fatty

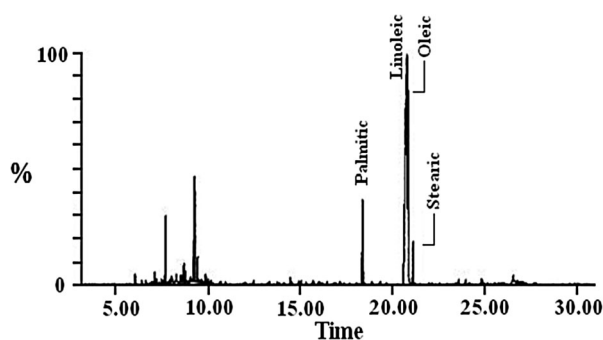


Figure 1. GC for MA-fatty acids methyl ester.

acids methyl ester was identified by comparison of retention indices (RI) in Figure 1, with chromatograms of standard fatty acid methyl esters (sigma, USA) and listed in Table 1.

From Table 1 it is obvious that the linoleic acid is the major constituent of mixed fatty acids of MA-oil. The average M Wt. of mixed fatty acids methyl ester for MA-Oil is 285.169.

2.2.2. Preparation of MA-amido surfactant

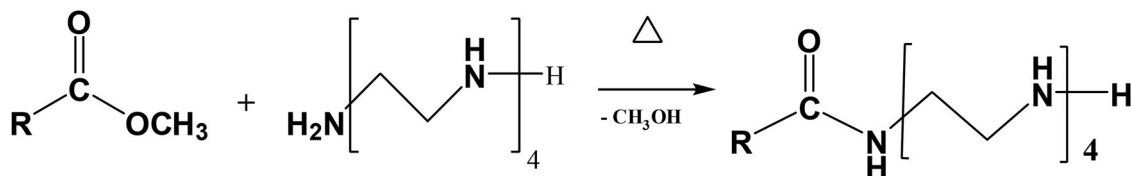
MA-amido surfactant was prepared by reacting equimolar amount of MA-fatty acids methyl ester (2.852 g, 0.01 M) with tetraethylenepentamine, $\text{NH}_2-(\text{CH}_2-\text{CH}_2-\text{NH})_4-\text{H}$ (1.89 g, 0.01 M), using fusion technique first at 80°C for 1 h and then raised to 110°C for 6 h (25) to give the product (3.801 g, yield 85.96%) as dark brown semisolid [Cf. Scheme 1]. The structure of the MA-amido surfactant was confirmed by FT-IR spectra by using a thermo Nicolet iS10 FT-IR spectrophotometer in the frequency range of 4000–400 cm^{-1} .

2.2.3. Determination critical micelle concentration of MA-amido surfactant

Critical micelle concentration (CMC) of MA-amido surfactant can be determined by measuring the surface tension of the synthesized MA-amido surfactant at a wide concentration range from 10^{-3} to 10^{-7} ML^{-1} with KRÜSS. TENSIO 10 METER K9. All diluted MA-amido surfactant solutions were prepared in bidistilled water with a surface tension equal to 72 mN m^{-1} at 25°C.

Table 1. Fatty acids’ composition of Egyptian *Melia azedarach* oil as a methyl ester.

Compounds	M (wt)	RI	Fatty acid (%)
Linoleic (C _{18:2})	294.513	20.85	62.52
Oleic (C _{18:1})	296.313	20.91	23.47
Stearic (C _{18:0})	298.513	21.17	03.42
Palmitic (C _{16:0})	270.459	18.45	07.87



Where : R - is the mixed alkyl fatty chain of MA fatty acids

Scheme 1.

2.3. Experimental methods

2.3.1. Gravimetric measurements

According to the ASTM, gravimetric corrosion measurements were performed (26). Rectangular steel specimens having dimensions of $(1.2 \times 1.1 \times 0.75)$ cm were immersed in 2.0 M HCl containing different concentrations of the synthesized MA-amido surfactant at different immersion times. The naturally aerated corrosive solution's temperature was 30°C. Each experiment was performed three times; there were small differences between the replicated experiments, indicating good reproducibility. For more data handling, the average of the measured three repeated values was used.

The corrosion rate ($\text{mg cm}^{-2} \text{min}^{-1}$) and the surface coverage (θ) and inhibition efficiency, η , were determined according to (18).

2.3.2. Electrochemical measurements

Electrochemical measurements were performed in a three-electrode cell with C-steel as working electrode, platinum as counter electrode and saturated calomel electrode as a reference electrode. The C-steel was mounted in Teflon with a geometric surface area of 0.32 cm^2 exposed to the electrolyte. The C-steel was mechanically abraded with a series of emery papers of (600) grade, up to the finest (1000) grade. Then the electrode was washed with bidistilled water and degreased with acetone immediately before insertion into the cell. Before each measurement, the electrode was allowed to corrode freely for 15 min to reach a quasi-stationary value of the open-circuit potential. PDP studies were performed using a Meinsberger potentiostat/Galvanostat with PS6 software for calculating the electrochemical parameters. The electrochemical parameters were obtained in 2.0 M HCl containing different concentrations of MA-amido surfactant at a scan rate of 1 mV sec^{-1} . The inhibition efficiency (η) and the fraction of surface coverage (θ) were calculated (17, 18).

EIS measurements were performed using a computer-controlled Princeton Applied Research PARSTAT 4000 teamed with the Versa Studio software package. The measurements were carried out with a frequency range

of 100 kHz to 10 MHz with a 10 mV sine wave as the excitation signal at open-circuit potential. Calculations of EIS parameters were performed as described previously (17, 18).

Every electrochemical experiment was performed three times to ensure the reliable and reproducible of the data; it was found quite acceptable reproducibility.

2.3.3. Scanning electron microscopy

The C-steel specimens were immersed in 2.0 M HCl solution in the absence and presence of 50 ppm MA-amido surfactant for 3 h at 30°C. After that the specimens were taken out and dried. The surface morphology of the C-steel samples in the absence and presence of MA-amido surfactant were investigated by using a FEI Quanta FEC 250 SEM microscope.

3. Results and discussion

3.1. Characterization of MA-amido surfactant

Figure 2(a,b) shows the FT-IR spectra of mixed fatty acids methyl ester of MA-oil and synthesized MA-amido surfactant $[\text{RCO}(\text{NH}-\text{CH}_2-\text{CH}_2)_4\text{NH}_2]$. It can be seen that the band of $\gamma \text{ C}=\text{O}$ in the mixed fatty acids methyl ester appears at 1743.18 cm^{-1} (Cf. Figure 2 (a)). While, the characteristic band of the $\gamma \text{ C}=\text{O}$ group of the amide surfactant appears at 1644.95 cm^{-1} (Cf. Figure 2 (b)). Moreover Figure 2 (b) shows the presence of two bands at 3205.88 cm^{-1} and 3416 cm^{-1} characteristic to $-\text{NH}_2$ group and repeating $-\text{NH}$ group moiety for the MA-amido surfactant, respectively (27).

3.2. Gravimetric measurements

3.2.1. Effect of immersion time

The WL experiments were carried out for C-steel in 2.0 M HCl solution containing different concentrations of MA-amido surfactant at different times of immersion. With respect to the WL measured, the degree of surface coverage (θ) was estimated, and then further inhibition efficiencies (η %) were calculated according to (17, 18). Figure 3(a,b) shows the dependence of both WL and

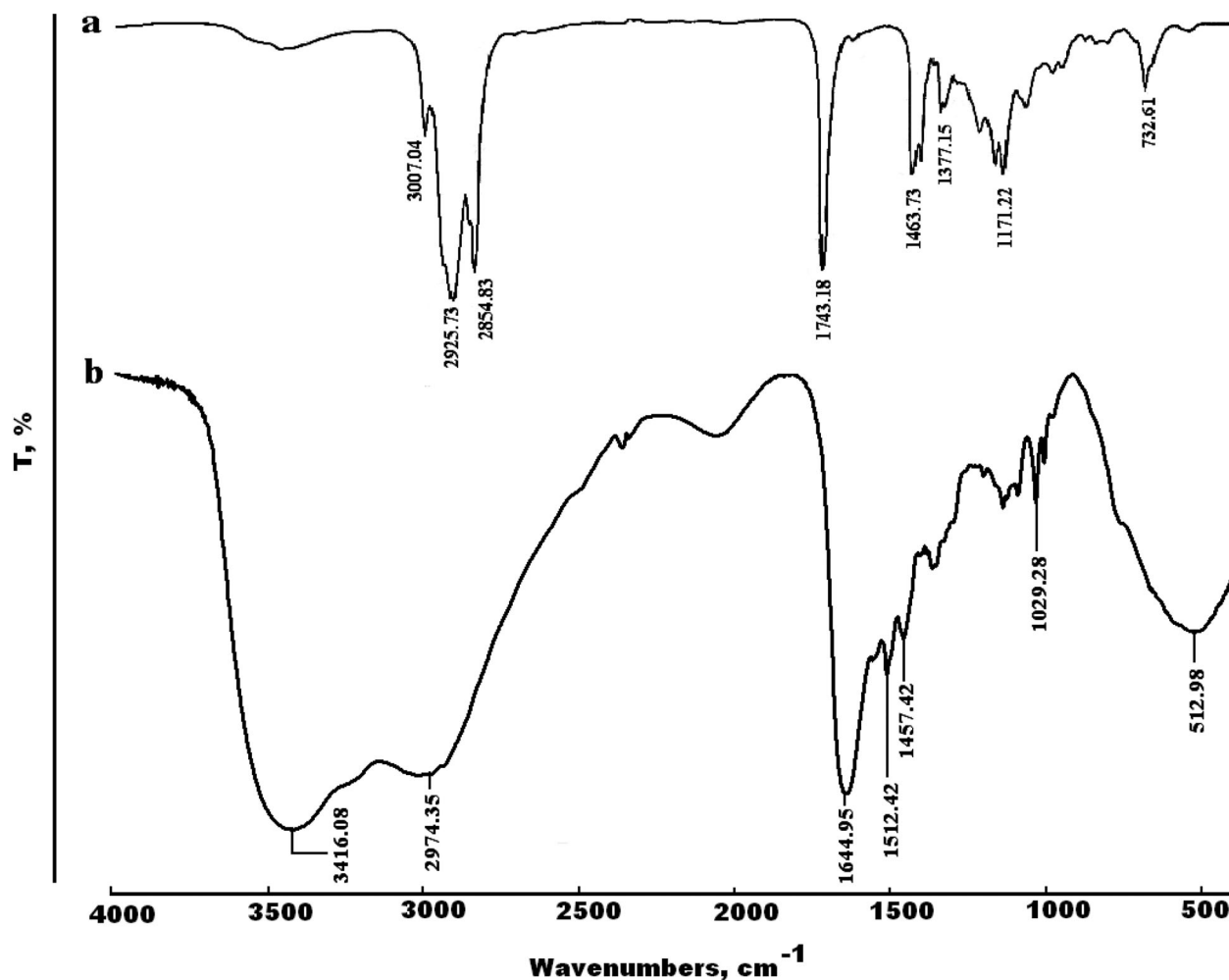


Figure 2. FT-IR of (a) mixed fatty acids methyl ester of MA-oil, (b) the MA-amido surfactant $\text{RCO}(\text{NH}-\text{CH}_2-\text{CH}_2)_4\text{NH}_2$.

inhibition efficiency on the exposure time, respectively. Inspection of Figure 3(a) reveals that WL of C-steel increased with increasing the immersion time in the absence and presence of MA-amido surfactant. This behavior can be attributed to the surface area of the studied C-steel sample not completely covered by the protective film (17). It is noticed from the figure that the presence of MA-amido surfactant effectively retards the corrosion rate of C-steel.

As depicted in Figure 3(a), the corrosion data fit the rate law for zero-order reaction as expressed (28, 29) in Equation (1):

$$\text{Weight loss} = k_0 t, \quad (1)$$

where k_0 is the zero-order rate constant and t is the corrosion time. The obtained linear plots with a correlation coefficient (R^2) of almost 1 confirm zero-order kinetics for the corrosion of the C-steel in 2.0 M HCl solution without and with the MA-amido surfactant. The calculated k_0 values from the slopes of Figure 3

(a) range from 0.01 to 0.0003, with increasing MA-amido surfactant concentrations. It is obvious that the k_0 decreases with an increase in MA-amido surfactant concentration, indicating an effective decrease in the dissolution rate of the C-steel in the acid solution. So the inhibition efficiency increases with increasing exposure time, as depicted in Figure 3(b). These results can be discussed in the view of, upon addition of the MA-amido surfactant in the corrosive medium, the additive molecules adsorbed randomly, at the first instant, at the C-steel surface. In this mode of adsorption, the molecules cannot arrange themselves properly on the steel surface. However, increasing the exposure time gave the chance for these adsorbed molecules to take their correct orientation toward the electrode when their hydrophilic part gets attached to the metal interface. Therefore, the hydrophobic parts oriented toward the aqueous solution, leading to push out the aggressive medium away from the metal surface. Thus, as the exposure time is increased,

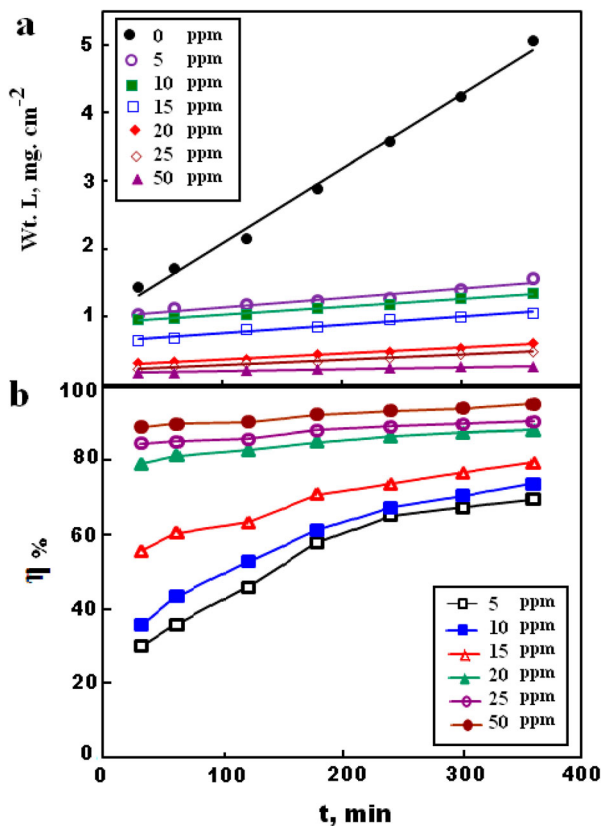


Figure 3. Relation between time of immersion for C-steel in 2.0 M HCl and (a) weight loss, (b) Inhibition efficiency, at different concentrations of MA-amido surfactant.

the arrangement of the adsorbed molecules increases, leading to an increase in the inhibition efficiency. From the results obtained, it can be seen that MA-amido surfactant is a good corrosion inhibitor for the C-steel in 2.0 M HCl.

3.2.2. Effect of inhibitor concentration

Figure 4 shows the inhibition efficiencies for the C-steel corrosion in 2.0 M HCl at different concentrations of MA-amido surfactant. The figure reveals that the inhibition efficiency is enhanced with the increase in MA-amido surfactant concentration. The maximum inhibition efficiency of approximately 95% is achieved at 50 ppm. This indicates that the adsorption process between the MA-amido surfactant and the C-steel surface is efficiently achieved and led to a strong metal-inhibitor interaction.

3.2.3. SEM analysis

SEM micrographs clear the changes that happened during the corrosion process of the polished C-steel before and after immersion in 2.0 M HCl along 3 h in the absence and presence of 50 ppm MA-amido surfactant as shown in Figure 5(a-c). Figure 5(a) shows the polished steel

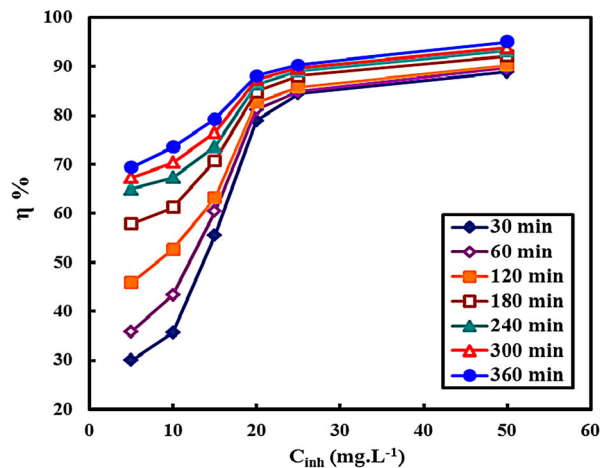


Figure 4. Relation between concentrations of MA-amido surfactant and inhibition efficiency at different immersion time.

surface before exposure to the corrosive media, where parallel scratches characteristic of the mechanical abrading are observed. The morphology of C-steel specimen on the surface was dramatically changed after exposure to the corrosive media in the absence of inhibitor as seen in Figure 5(b) due to rapid corrosion attack. But, the deterioration of the metal is more clearly reduced in the presence of MA-amido surfactant, even the polishing lines can be observed under the aggregation of the surfactant molecules, as shown in Figure 5(c). This observation clearly proves that MA-amido surfactant can form an effective protective film and hence show good inhibiting ability at the C-steel surface.

3.2.4. Adsorption isotherm

Organic inhibitors get adsorbed onto the metal surface through physical and/or chemical bonds so as to form a protective layer. The extent of the protective layer depends on the chemical structures of adsorbed compounds, hydrophobic nature of the protective barrier which prevent the exchange of the electrical charge and the substance migration and the nature of aggressive media (30).

Surface coverage (θ) at different concentrations of MA-amido surfactant was calculated from the WL measurements in 2.0 M HCl at 30°C for 6 h of immersion period. The data were tested graphically by fitting to various adsorption isotherms. The correlation coefficient (R^2) was used to find the best fit isotherm which was obtained. Figure 6 shows the straight line obtained by the plot of C/θ against C , with a linear correlation and the slope close to unity confirms the obeying of Langmuir isotherm. According to this isotherm, θ is related to the inhibitor concentration according to the following

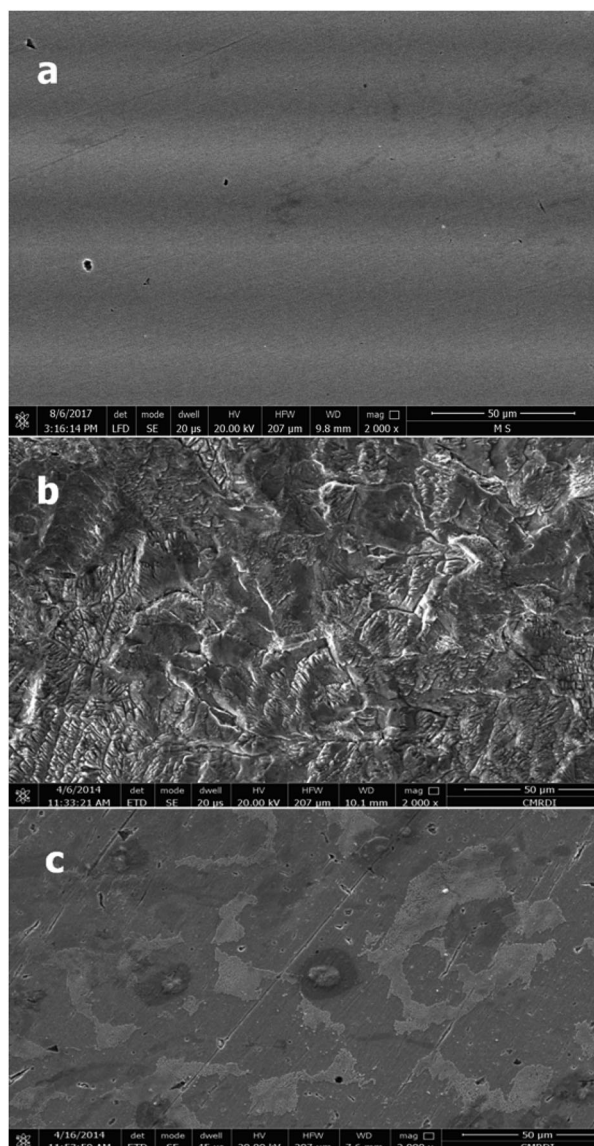


Figure 5. SEM micrograph (2000 X) of C-steel surface: (a) polished surface of metal, (b) polished C-steel immersed in 2.0 M HCl after 3 h, (c) polished C-steel immersed in 2.0 M HCl containing 50 ppm of MA-amido surfactant after 3 h.

equation (18, 31):

$$\frac{C_{\text{inh}}}{\theta} = \frac{1}{K_{\text{ads}}} + C_{\text{inh}}, \quad (2)$$

where θ is the surface coverage, C is the concentration of inhibitor, and K_{ads} is the equilibrium adsorption constant.

The adsorptive constant of equilibrium (K_{ads}) is related to the standard adsorption free energy (ΔG°) according to (18):

$$K_{\text{ads}} = \left(\frac{1}{C_{\text{solvent}}} \right) e^{-\Delta G_{\text{ads}}/RT}, \quad (3)$$

where C_{solvent} is the concentration of water in solution. The unit of K_{ads} is (l mg^{-1}), which results in that the

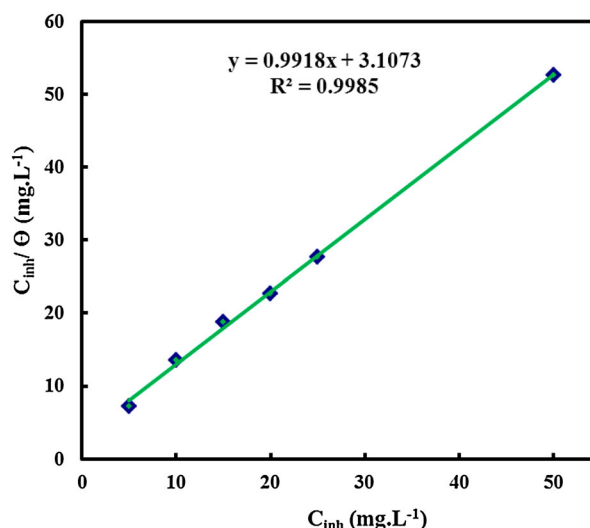


Figure 6. Langmuir adsorption isotherm.

unit of C_{solvent} is mg l^{-1} with the value of approximate 1×10^6 .

In general, values of the free energy of adsorption ΔG_{ads} , up to -20 kJ mol^{-1} seemed to suggest the electrostatic interaction between the charged molecules and the charged metal (physical adsorption), while those higher than -40 kJ mol^{-1} involved charge sharing or transfer from the inhibitor molecules to the metal surface to form a co-ordinate type of bond (chemisorption) (19). The obtained value of ΔG_{ads} is equal to $-31.44 \text{ kJ mol}^{-1}$, which suggests a spontaneous physico-chemical adsorption mechanism of MA-amido surfactant at the carbon steel surface in 2.0 M HCl.

3.3. PDP studies

3.3.1. Effect of MA-amido surfactant concentration

Figure 7 shows the anodic and cathodic polarization curves of C-steel in 2.0 M HCl, free and containing different concentrations of MA-amido surfactant. It is clear that the addition of MA-amido surfactant has an inhibiting effect in both anodic and cathodic parts of the polarization curves and shifts them to lower current densities. These results are attributed to adsorption of the MA-amido surfactant at the C-steel surface.

The corrosion parameters extracted from the polarization curves such as, the values of the corrosion current densities (i_{corr}), the corrosion potential (E_{corr}), the cathodic (β_c) and anodic Tafel (β_a) slopes were obtained by extrapolation of anodic and cathodic regions of the Tafel plots and are reported in Table 2.

Inspection of Table 2 shows that increasing MA-amido surfactant concentrations shift the corrosion potential (E_{corr}) of C-steel in corrosive medium toward less negative

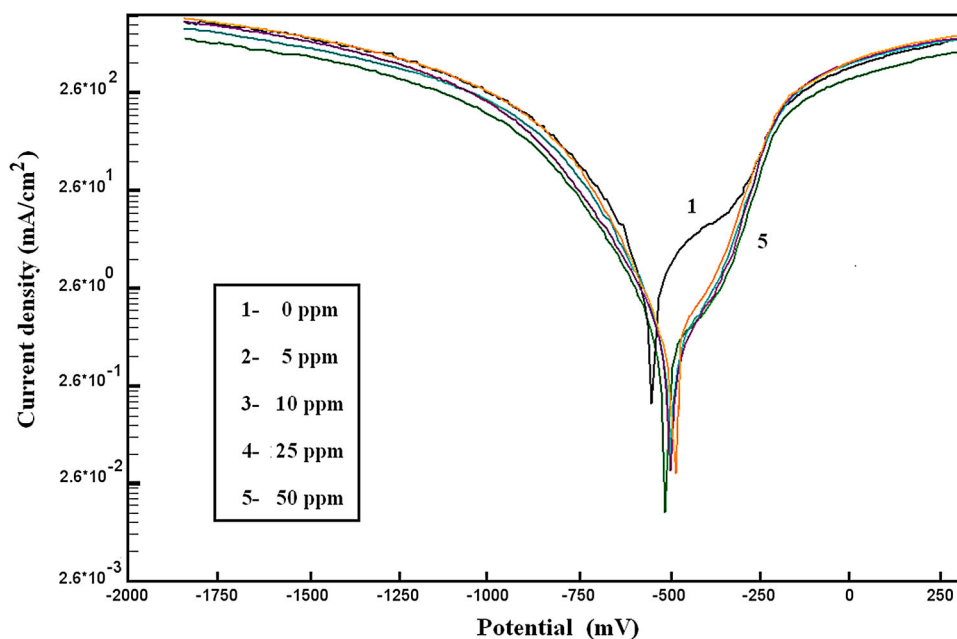


Figure 7. Anodic and cathodic polarization curves of C-steel in 2.0 M HCl containing different concentrations of MA-amido surfactant.

values of about 65 mV. Both cathodic β_c and anodic β_a tafel slopes are decreased; however, the anodic Tafel slope β_a decreased more than the cathodic one. In addition, the values of corrosion current densities (i_{corr}) were decreased to a greater extent. The corresponding inhibition efficiencies increase to reach approximately, 86%. These results indicate that the MA-amido surfactant acts as a mixed-type inhibitor with predominant anodic effectiveness, retards anodic dissolution and reduces the cathodic hydrogen evolution reaction (32, 33). These results can be attributed to the formation of ferrous ions due to anodic dissolution of C-steel in a strong acid medium, thus, enabling the unshared electron pair on nitrogen atoms of the prepared amide compound to coordinate with the freshly produced Fe (II) species and form an insoluble Fe (II)-inhibitor complex (34) that protects the metal from the aggressive media.

3.3.2. Effect of temperature

The effect of temperature at the C-steel corrosion in 2.0 M HCl solution free and containing 50 ppm of MA-

amido surfactant at temperature ranging from 30°C to 60°C was studied by PDP technique. The kinetic parameters obtained from Tafel plots for C-steel in 2.0 M HCl in the absence and presence of 50 ppm of the MA-amido surfactant at different temperature were given in Table 3.

Inspection of Table 3 reveals that the corrosion current density of C-steel in both free and inhibited acid media increased as the temperature was increased. It is obvious that the presence of the tested inhibitor retarded the dissolution of C-steel extensively. The inhibition efficiency of the MA-amido surfactant is not affected by the rise of temperature from 30°C to 60°C.

3.3.3. Thermodynamics parameters

A plot of $\log i_{corr}$ (mA cm^{-2}) of C-steel obtained from Tafel plots vs. $1/T$ gave straight lines, as shown in Figure 8(a); the apparent activation energies (E_a) were calculated by using an Arrhenius-type equation (34, 35):

$$\log i_{corr} = \log A - \frac{E_a}{2.303RT}, \quad (4)$$

where i_{corr} is the current density (mA cm^{-2}), A is the frequency factor, E_a is the apparent activation energy and R is the molar gas constant.

The values of E_a are listed in Table 4. As seen in Table 4, the value of apparent activation energy in the presence of 50 ppm of MA-amido surfactant is larger than that of the uninhibited aggressive solution. The obtained result ensures the formation of protective

Table 2. Kinetic parameters obtained from Tafel plots for C-steel in 2.0 M HCl in the absence and presence of MA-amido surfactant.

C (ppm)	E_{corr} (mV)	i_{corr} (mA cm^{-2})	β_a (mV dec^{-1})	β_c (mV dec^{-1})	η (%)
0	-528	1.060	204	-183	-
5	-463	0.360	109	-183	66.04
10	-453	0.230	106	-181	78.30
25	-465	0.190	107	-148	82.08
50	-463	0.147	109	-147	86.13

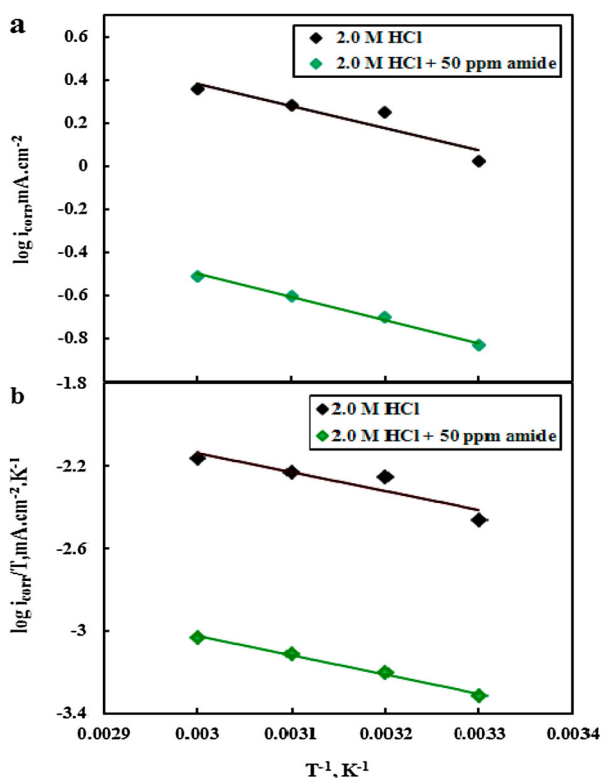
Table 3. Kinetic parameters obtained from Tafel plots for C-steel in 2.0 M HCl in the absence and presence of 50 ppm of the prepared MA-amido surfactant at different temperature.

Temp (K)	Solution	E_{corr} (mV)	i_{corr} (mA cm ⁻²)	η (%)	β_a (mV dec ⁻¹)	β_c (mV dec ⁻¹)
303	Free	-528	1.060	-	204	-183
	Inhibited	-463	0.147	86.13	109	-147
313	Free	-528	1.780	-	120	-199
	Inhibited	-468	0.200	88.76	120	-166
323	Free	-550	1.920	-	136	-165
	Inhibited	-438	0.250	86.98	123	-194
333	Free	-548	2.292	-	150	-190
	Inhibited	-448	0.310	86.47	144	-188

MA-amido surfactant film at the C-steel surface, which retard the mass and energy transfer.

Thermodynamic parameters for corrosion of C-steel in 2.0 M HCl devoid of and containing 50 ppm of the MA-amido surfactant are calculated from the transition state equation (18):

$$i_{\text{corr}} = \frac{RT}{Nh} \exp\left(\frac{\Delta S^*}{R}\right) \exp\left(\frac{-\Delta H^*}{RT}\right), \quad (5)$$

**Figure 8.** Arrhenius plots (a) and transition state plots (b) of C-steel in 2.0 M HCl in the absence and presence of 50 ppm MA-amido surfactant.**Table 4.** The values of the activation parameters for C-steel in 2.0 M HCl in the absence and presence of different concentrations of MA-amido surfactant.

Medium	E_a (kJ mol ⁻¹)	ΔH^* (kJ mol ⁻¹)	ΔS^* (J mol ⁻¹ K ⁻¹)
Free	19.86	17.62	-185.63
Inhibited	20.43	18.04	-201.31

where N is the Avogadro number, h is the Planck constant and ΔS^* , ΔH^* is the entropy and enthalpy of activation respectively. Plot of $\log(i_{\text{corr}}/T)$ vs. $1/T$, Figure 8 (b), gave straight lines with slope equal $(-\Delta H^*/2.303R)$ and an intercept equal $(\log R/Nh + \Delta S^*/2.303R)$. The values of ΔS^* and ΔH^* were calculated and tabulated in Table 4.

Inspection of Table 4 shows that, the values of E_a are greater than the analogous values of ΔH^* , indicating that the corrosion process must involve a gaseous reaction, simply the hydrogen evolution reaction (35). The calculated value of the $E_a - \Delta H^*$ was 2.40 kJ mol⁻¹. This value was compatible with RT value at room temperature (2.63 kJ mol⁻¹). This ensures the unimolecular character of the corrosion process according to the following equation (31, 35):

$$E_a - \Delta H^* = nRT. \quad (6)$$

Also, it is clear from the table that the value of ΔH^* in presence of MA-amido surfactant is higher than that in free solution, indicating higher protection efficiency for C-steel. The positive sign of activated enthalpy (ΔH^*) means the endothermic nature of the C-steel corrosion (36). High negative values of ΔS^* proves that the activated complex shows an association more than a dissociation, in the rate-determining step. This means a decrease in disorder occurred as the reaction proceeds from reactants to the activated complex (7, 36). The more negative values of the ΔS^* in inhibiting solution can be interpreted that the MA-amido surfactant molecules involved in the activated complex of the corrosion reaction lead to more ordered systems.

3.4. The EIS

EIS is an important technique to study the corrosion protection of metals at different concentrations of testing inhibitor compounds, and gives data about the resistance and capacitance behavior at the interface between an electrode and its surrounding electrolyte. Figure 9(a-c) represents Nyquist, $\log(f) - \log|Z|$, and Bode phase plots of the C-steel electrode in 2.0 M HCl

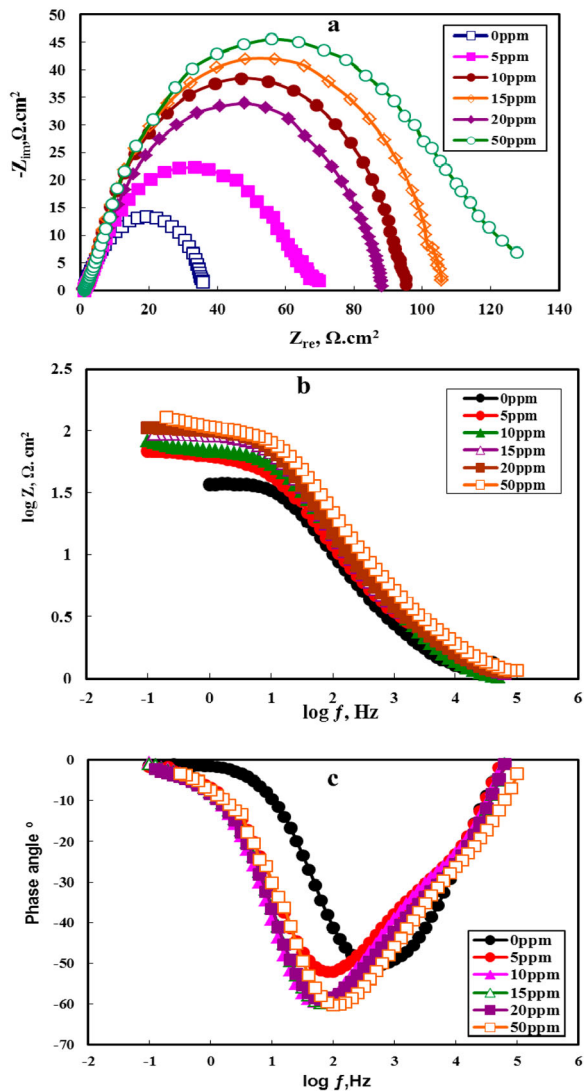


Figure 9. Nyquist plots (a), Bode plots (b) and Bode phase plots (c) for C-steel in 2.0 M HCl containing different concentrations of MA-amido surfactant.

solution in the absence and presence of different concentrations of MA-amido surfactant, respectively. Figure 9(a,b) shows that, the Nyquist plot of C-steel in the absence and presence of the MA-amido surfactant contains a slightly depressed semi-circular shape and only one time constant appears in $\log(f) - \log|Z|$ plot, which indicates that the charge transfer process is

the essential controller of the corrosion of C-steel in 2.0 M HCl media. The Nyquist plots' deviation from ideal state of semi-circle is due to the frequency dispersion and inhomogeneities of the surface (18). However, the increasing in Nyquist plots diameter after adding the MA-amido surfactant to the corrosive solution clearly shows an improvement in the metal corrosion resistance. Figure 8(c) shows that, increasing the concentration of MA-amido surfactant in 2.0 M HCl causes changes for phase angle toward more negative values, indicating better inhibiting behavior due to the adsorption of more MA-amido surfactant molecules on the metal surface at high concentrations (18). It is obvious from Figure 9 that the presence of the MA-amido surfactant in the corrosive solution does not affect the appearance of impedance plots, which suggests a similar mechanism for the C-steel corrosion.

The ideal capacitors must have a slope (α) with a value of -1 at the linear region of the $\log(f) - \log|Z|$ plots. The experimental α value is calculated from the $\log(f) - \log|Z|$ plots given in Table 5. Inspection of Table 5 reveals that α values ranged from -0.57 to -0.72 , which is related to the non-ideal structure of the double layer. In this case, a differential capacitance is set up at the interface between an electrode and its surrounding electrolyte. This is often referred to frequency dispersion as a result of the non-homogeneity or the roughness of the solid surface. After the addition of amide, α value increasing towards the ideal value (-1) indicates decreasing the surface inhomogeneity as a result of the inhibitor molecules adsorption at the C-steel surface.

Based on the findings of impedance plots, a simple Randles electrical equivalent circuit diagram was used to model the steel/solution interface as described before (17, 18). The related fitting parameters are given in Table 5. They include a solution resistance R_s , constant phase element (CPE) which is related to the capacity of the electrical double layer (C_{dl}), and a charge transfer resistance R_{ct} . For more fitting accuracy, the double layer capacitance (C_{dl}) was replaced by the impedance of CPE according to (18, 34):

$$Z_{CPE} = Q^{-1}(j\omega)^{-\alpha}, \quad (7)$$

Table 5. Impedance parameters and inhibition efficiency of C-steel in 2.0 M HCl solution in the absence and presence of investigated inhibitor.

C (ppm)	R_s ($\Omega \text{ cm}^2$)	R_{ct} ($\Omega \text{ cm}^2$)	f_{max} (Hz)	$Q \times 10^{-3}$ ($\text{s}^\alpha \Omega^{-1} \text{ cm}^{-2}$)	C_{dl} (F cm^{-2})	α	η (%)
0	1.68	34.58	50.12	27.1	25.60	-0.57	-
5	1.16	68.55	31.62	14.3	14.10	-0.58	49.56
10	1.18	83.82	25.12	11.3	11.00	-0.59	58.75
15	1.10	94.14	10.00	10.0	10.00	-0.65	63.27
20	1.13	104.50	7.94	9.50	9.40	-0.69	66.91
50	1.17	136.00	6.30	7.30	7.28	-0.72	74.57

where Q is the admittance factor have the unit of $s^{\alpha} \Omega^{-1} \text{cm}^{-2}$, $j^2 = -1$, and ω is the angular frequency in rad^{-1} ($\omega = 2\pi f_{\text{max}}$, f_{max} is the frequency at maximum imaginary component of the impedance) and α is a CPE exponent.

The adsorption capacitance is calculated according to the following equation (36, 37):

$$C_{\text{dl}} = (QR_{\text{ct}}^{1-\alpha})^{1/\alpha}. \quad (8)$$

The fitting data in Table 5 shows that R_{ct} values increased with the increasing inhibitor concentration, which indicates the enhancement of surface coverage by the inhibitor molecules leading to increase the inhibition of C-steel corrosion (18). However, the capacitance (C_{dl}) values were decreased with the increasing inhibitor concentration, which indicates the extended adsorption of inhibitor molecules monolayer at the metal surface to offer better surface coverage and/or the enhancement the thickness of the protective layer at the metal/solution interface (18, 37). In other words, the decrease of capacitance is due to the displacement of water molecules and other ions originally adsorbed at the electrode surface by the MA-amido surfactant molecules to form a protective layer which decreases the number of active sites necessary for the corrosion reaction and so increases corrosion inhibition and/or increasing the double layer thickness of adsorbed MA-amido surfactant molecules as Helmholtz model stated (36, 37):

$$C_{\text{dl}} = \frac{\epsilon \epsilon_0}{\delta} S, \quad (9)$$

where δ is the thickness of the protective layer, S is the surface of the used electrode, ϵ_0 is the permittivity of the air and ϵ is the dielectric constant of medium.

It was noticed from the Table 5 that C_{dl} values are decreased in the presence of the inhibitor more than in its absence due to the effective adsorption of the MA-amido surfactant.

It is apparently seen that, the WL experiments achieve better inhibition efficiencies than those obtained by electrochemical one due to their different exposure time period.

3.5. Surface properties of MA-amido surfactant

3.5.1. CMC of surfactant

CMC can be determined experimentally by measuring surface tension (γ) at different concentrations of the MA-amido surfactant. The obtained surface tension values are plotted as a function of the logarithm of the surfactant concentration as depicted in Figure 10. The figure shows two characteristic regions, the first section of the curve at lower concentrations is featured by a

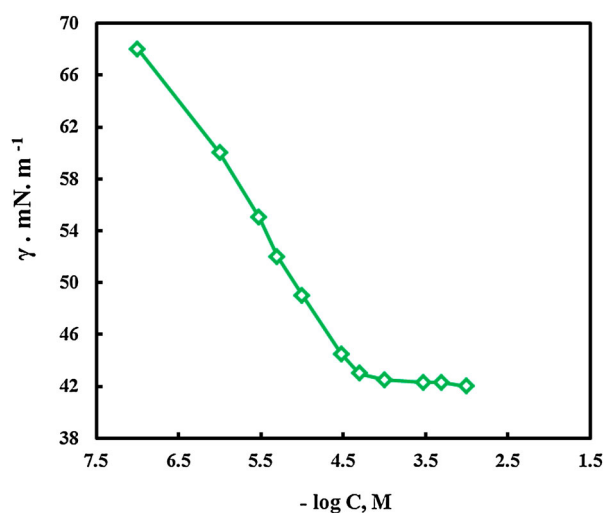


Figure 10. Surface tension-concentration profile of MA-amido surfactant at 25°C.

continuous decrease in the surface tension values owing to the adsorption of surfactant molecules at water interface. In the second section, the surface tension is nearly constant at high surfactant concentrations. The break point in the resulting curve clarifies the concentration at which the micelles were formed (the CMC) (38).

At CMC, water interface can be fully covered by MA-amido molecules. After CMC, MA-amido surfactant molecules are accumulated forming the micelles (39).

3.5.2. Effectiveness (π_{CMC})

The effectiveness (π_{CMC}) of the tested surfactant is calculated from the following equation (39):

$$\pi_{\text{CMC}} = \gamma_0 - \gamma_{\text{CMC}}, \quad (10)$$

where γ_0 , γ_{CMC} are the surface tension measured for pure water and at CMC, respectively, at 25°C. The calculated values are listed in Table 6.

3.5.3. Surface excess (Γ_{max})

The effective measure of the surfactant adsorption at the air/water interface is expressed as surface excess, Γ_{max} . The surface excess (Γ_{max}) value for prepared surfactant is determined according to the Gibbs adsorption equation (38, 40) and recorded in Table 6:

$$\Gamma_{\text{CMC}} = \left(\frac{-1}{2.303RT} \right) \left(\frac{\partial \gamma}{\partial \log C} \right), \quad (11)$$

Table 6. Surface properties of MA-amido surfactant.

CMC (M)	γ_{CMC} (mN m ⁻¹)	π_{CMC} (mN m ⁻¹)	Γ_{max} (Mol Cm ⁻²)	A_{min} (nm ²)	$\Delta G_{\text{mic}}^{\circ}$ (kJ mol ⁻¹)
5.01×10^{-5}	43	29	1.67×10^{-10}	99.44	-25

where $(\partial\gamma/\partial \log C)$ is the slope of the surface tension – $\log C$ curve at the pre-micelle region and C is the MA-amido surfactant concentration.

3.5.4. Minimum surface area (A_{min})

The minimum average area (A_{min}) occupied by surfactant molecules at the aqueous-air interface can be calculated according to (40):

$$A_{min} = (10^{16}/N_A\Gamma_{max}), \quad (12)$$

where N_A is Avogadro's number ($6.022 \times 10^{23} \text{ mol}^{-1}$).

A_{min} is listed in Table 6. The small value of A_{min} proposed that the MA-amido surfactant molecules at water/air interface are close-packed; therefore, the orientation of the MA-amido surfactant molecule at the interface was nearly perpendicular at CMC value.

3.5.5. The standard free energy of micelle formation

ΔG_{mic}°

ΔG_{mic}° can be calculated according to (38):

$$\Delta G_{mic}^\circ = RT \ln (C_{CMC}/\text{mol L}^{-1}). \quad (13)$$

The calculated ΔG_{mic}° is recorded in Table 6. The negative value of ΔG_{mic}° measure a spontaneous tendency of the synthesized surfactant to form micelles.

3.6. Determination of CMC of MA-amido surfactant from corrosion parameters

CMC can be determined using the corrosion kinetic parameters through another form of the Langmuir isotherm according to (41):

$$\frac{1}{C_R} = (K^- + KC), \quad (14)$$

where C_R is the corrosion rate, K is the adsorption equilibrium constant, K^- is the inverse of the corrosion rate in absence of inhibitor and, C is MA-amido surfactant concentration.

Figure 11 represents the variation of θ versus different concentration of MA-amido surfactant in 2.0 M HCl using WL, potentiodynamic and EIS techniques, where θ values ($\eta \% 100$) is related to the corrosion rate according to (17, 18). It is obvious from the figure that, the tested techniques gave three identical curves. Each curve has two slopes; the first slope was more severe below the CMC, while the second slope decreased after the CMC. This result was attributed to the adsorption conversion from traditional Langmuir monolayer-level to multilayer adsorption. It was noted that, the intersections of the two straight lines in each curve were recorded at the same value at exactly $C = 20 \text{ ppm}$ ($4.52 \times 10^{-5} \text{ M}$), which corresponds to CMC value of MA-amido surfactant

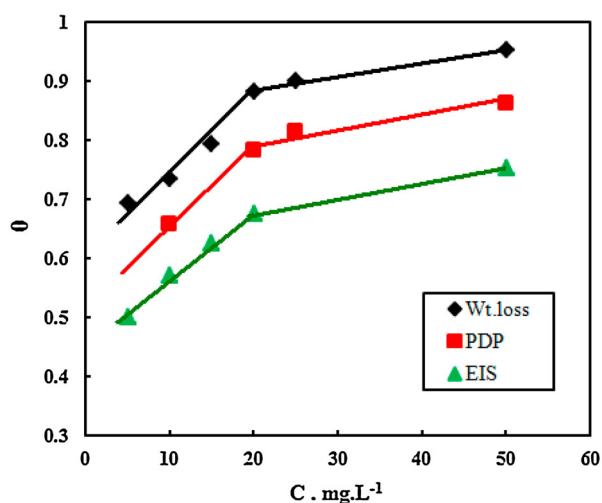


Figure 11. Plot of the surface coverage θ vs. different concentrations of added MA-amido surfactant.

(41). The variation in the ionic strength between hydrochloric acid and pure water is responsible for the noted difference in the CMC (41).

4. Mechanism of adsorption

Owing to the chemical structure of the MA-amido surfactant, acidic nature of the studied medium and the positively charged surface of the C-steel, the adsorption may occur through two modes, physical and chemical adsorption (see Section 3.2.4).

The MA-amido surfactant exists in the studied acidic media either as neutral and/or cationic molecules. The adsorption of MA-amido surfactant molecules occurs at the C-steel/acid solution interface via one or more of the following ways;

- (1) interaction between the unshared electron pairs of nitrogen atoms in the MA-amido surfactant and the vacant d-orbital of iron atoms, causing the adsorption of the neutral MA-amido surfactant via the chemisorption mechanism. In turn, the adsorption of MA-amido surfactant leads to both the replacement of water molecules by organic molecules and a decrease in the potential of chloride ion (Cl^-) attack at the C-steel surface.
- (2) in the acidic media, the amino and/or $-\text{NH}_2$ groups of the MA-amido surfactant may be protonated, creating a positive charge on the surfactant molecules. Simultaneously, C-steel surface carries a positive charge in the acidic solution (H_3O^+ / metal interface) due to Antropov's rational corrosion potential (42), thus favors the static interaction with the negatively charged Cl^- ions. Therefore, the

positively charged MA-amido surfactant molecules can physically adsorb to the positively charged metal surface through electrostatic interactions by using chloride ions as a negative bridge. Such synergism behavior between adsorbed Cl^- ions and protonated inhibitor molecules is established to achieve efficient adsorption. In turn, the formed positively protective film of the inhibitor repels away electrostatically the H^+ ions of the corrosive media and therefore decreases the corrosion rate.

Generally the inhibition efficiency of MA-amido surfactant depends on:

- (1) its adsorption at the C-steel surface via the hydrophilic head groups, amino and/or $-\text{NH}_2$ groups, at different concentration of the MA-amido surfactant forming mono- or multilayer that shielding the C-steel from the corrosive media and hence decreasing the corrosion rate (see Figures 4 and 11).
- (2) on the other hand, the organic character of the hydrophobic chain (lyophile) in MA-amido surfactant molecules increases the repulsion of the aqueous phase away from the metal surface (43). Consequently, the amphipathic structure of the MA-amido surfactant is responsible for its high inhibition efficiency.

5. Conclusion

- (1) The MA-amido surfactant acts as good corrosion inhibitors for C-steel in 2.0 M HCl solution, and its inhibition efficiency is increased with increasing the concentration.
- (2) The inhibition efficiency was slightly constant as the temperature was increased from 30°C to 60°C
- (3) The value of ΔG° suggested that MA-amido surfactant adsorbed at the C-steel surface due to physical and chemical adsorption. The adsorption process is spontaneous and followed Langmuir adsorption isotherm model.
- (4) PDP results revealed that MA-amido surfactant suppress both cathodic and anodic polarization reactions.
- (5) SEM images suggest that, MA-amido surfactant form protective film at the surface of C-steel specimen in 2.0 M HCl.

Acknowledgement

The authors wish to thank all the staff members at Chemistry Department, Faculty of Science, Benha University, Egypt for their cooperation.

Disclosure statement

No potential conflict of interest was reported by the authors.

Notes on contributors

Dr. Asmaa. A.I. Ali, born in 1976, achieved her PhD in physical Chemistry in 2008. She is a lecturer at Chemistry Dept., faculty of science in Benha University, Egypt. Her research interests are in the fields of corrosion protection of metals.

Prof. Wagdy I.A. El-Dougdoug, born in 1964, achieved his PhD in Organic Chemistry in 1995. He is a Professor at Chemistry Dept., faculty of Science, Benha University, Egypt. He is Executive Director of Quality Assurance at faculty of Science, Benha University, Egypt. His research interests are in the fields of surfactants.

References

- [1] El-Meligi, A.A.; Turgoose, S.; Ismael, A.A.; Sanad, S.H. *Br. Corros. J.* **2000**, *35* (1), 75–77.
- [2] Saha, S. Kr.; Dutta, A.; Ghosh, P.; Sukul, D.; Banerjee, P. *Phys. Chem. Chem. Phys.* **2015**, *17*, 5679–5690.
- [3] Saha, S. Kr.; Dutta, A.; Ghosh, P.; Sukul, D.; Banerjee, P. *Phys. Chem. Chem. Phys.* **2016**, *18*, 17898–17911.
- [4] El-Faham, A.; Osman, S.M.; Al-Lohedan, H.A.; El-Mahdy, G.A. *Molecules.* **2016**, *21*, 714–727.
- [5] Peme, T.; Olanakanmi, L.; Bahadur, I.; Adekunle, A.S.; Kabanda, M.M.; Ebenso, E.E. *Molecules.* **2015**, *20*, 16004–16029.
- [6] Pradeep Kumar, C.B.; Mohana, K.N. *J. Taiwan Inst. Chem. Eng.* **2014**, *45*, 1031–1042.
- [7] Shahabi, S.; Norouzi, P.; Ganjali, M.R. *RSC Adv.* **2015**, *5*, 20838–20847.
- [8] Solmaz, R. *Corros. Sci.* **2014**, *79*, 169–176.
- [9] Abd El-Lateef, H.M.; Tantawy, A.H. *RSC Adv.* **2016**, *6*, 8681–8700.
- [10] Ostapenko, G.; Gloukhov, P.; Bunev, A. *ECS Trans.* **2013**, *53* (33), 41–48.
- [11] Motamedi, M.; Tehrani-Bagha, A.R.; Mahdavian, M. *Corros. Sci.* **2013**, *70*, 46–54.
- [12] Sobhi, M.; El-Sayed, R.; Abdallah, M. *Chem. Eng. Commun.* **2016**, *203*, 758–768.
- [13] Al-Senani, G.M. *Int. J. Electrochem. Sci.* **2016**, *11*, 291–302.
- [14] Verma, D.K.; Khan, F. *Green Chem. Lett. Rev.* **2016**, *9* (1), 52–60.
- [15] Gadow, H.S.; Motawea, M.M. *RSC Adv.* **2017**, *7*, 24576–24588.
- [16] Gadow, H.S.; Fouda, A.S. *Int. J. Adv. Res.* **2014**, *2* (1), 233–243.
- [17] El-Etre, A.Y.; Ali, A.I. *Chin. J. Chem. Eng.* **2017**, *25*, 373–380.
- [18] Ali, A.I.; Mahrous, Y.Sh. *RSC Adv.* **2017**, *7*, 23687–23698.
- [19] Tawfik, S.M. *RSC Adv.* **2015**, *5*, 104535–104550.
- [20] Raja, P.B.; Qureshi, A.K.; Abdul Rahim, A.; Osman, H.; Awang, K. *Corros. Sci.* **2013**, *69*, 292–301.
- [21] Bost, R.W.; Fore, D.J. *Mitchell Soc.* **1935**, 134–142.
- [22] Morrison, R.T.; Boyd, R.N. *Organic Chemistry*, 6th ed.; Prentice Hall International united states, **1992**.
- [23] El-Sawy, A.A. *Grasas y Aceites.* **1989**, *40*, 382–384.
- [24] Abo-Riya, M.; Tantawy, A.H.; El-Dougdoug, W. *J. Mol. Liq.* **2016**, *221*, 642–650.
- [25] El-Dougdoug, W.I.A. *Grasas y Aceites.* **1999**, *50* (5), 385–391.

- [26] ASTM, *Standard Practice for Laboratory Immersion Corrosion Testing of Metals*, G 31–72; ASTM: Philadelphia, PA, 1990; p. 401.
- [27] Bellamy, L.J. *The Infra-red Spectra of Complex Molecules*, 3rd ed.; Chapman & Hall: London, 1975.
- [28] Abiola, O.K.; Otaigbe, J.O.E. *Int. J. Electrochem. Sci.* **2008**, *3*, 191–198.
- [29] Engel, T.; Reid, P. *Physical Chemistry*, 1st ed.; Pearson Education: New Delhi, 2006.
- [30] Xinkuai, H.; Yumei, J.; Chen, L.; Weichun, W.; Bailong, H.; Luye, W. *Corros. Sci.* **2014**, *83*, 124–136.
- [31] Ali, A.I. *J. Mater. Environ. Sci.* **2014**, *5* (3), 793–802.
- [32] Shaban, S.M.; Aiad, I.; El-Sukkary, M.M.; Soliman, E.A.; El-Awady, M.Y. *J. Mol. Liq.* **2015**, *203*, 20–28.
- [33] Shaban, S.M. *RSC Adv.* **2016**, *6*, 39784–39800.
- [34] Ahamad, I.; Prasad, R.; Quraishi, M.A. *Corros. Sci.* **2010**, *52*, 1472–1481.
- [35] Ali, A.I.; Megahed, H.E.; El-Etre, M.A.; Ismail, M.N. *J. Mater. Environ. Sci.* **2014**, *5* (3), 923–930.
- [36] Zheludkevich, M.L.; Yasakau, K.A.; Poznyak, S.K.; Ferreira, M.G.S. *Corros. Sci.* **2005**, *47*, 3368–3383.
- [37] Macdonald, J.R. *Impedance Spectroscopy*, John Wiley & Sons: New York, 1987.
- [38] Tawfik, S.M.; Sayed, A.; Aiad, I. *J. Surfact. Deterg.* **2012**, *15*, 577–585.
- [39] Negm, N.A.; Mahmoud, S.A. *Egypt J. Petrol.* **2003**, *20*, 1211.
- [40] Rosen, M.J. *Surfactants and Interfacial Phenomena*, 2nd ed.; Wiley: New York, 1992.
- [41] Fuchs-Godec, R. *Colloids Surf. A Physicochem. Eng. Aspects.* **2006**, *280*, 130–139.
- [42] Lebrini, M.; Lagrenee, M.; Traisnel, M.; Gengembre, L.; Vezin, H.; Bentiss, F. *Appl. Surf. Sci.* **2007**, *253*, 9267–9276.
- [43] Motamedi, M.; Tehrani-Bagha, A.R.; Mahdavian, M. *Prog. Org. Coat.* **2014**, *77*, 712–718.